

## Reduced-order modeling based on POD of a parabolized Navier–Stokes equation model I: forward model

J. Du<sup>1,2</sup>, I. M. Navon<sup>2,\*</sup>,†, J. L. Steward<sup>2</sup>, A. K. Alekseev<sup>3</sup> and Z. Luo<sup>4</sup>

<sup>1</sup>*School of Science, Beijing Jiaotong University, Beijing 100044, China*

<sup>2</sup>*Department of Scientific Computing, Florida State University, Tallahassee, FL 32306-4120, USA*

<sup>3</sup>*Moscow Institute of Physics and Technology, Moscow 141700, Russia*

<sup>4</sup>*School of Mathematics and Physics, North China Electric Power University, Beijing 102206, China*

### SUMMARY

A proper orthogonal decomposition (POD)-based reduced-order model of the parabolized Navier–Stokes (PNS) equations is derived in this article. A space-marching finite difference method with time relaxation is used to obtain the solution of this problem, from which snapshots are obtained to generate the POD basis functions used to construct the reduced-order model. In order to improve the accuracy and the stability of the reduced-order model in the presence of a high Reynolds number, we applied a Sobolev  $H_1$  norm calibration to the POD construction process. Finally, some numerical tests with a high-fidelity model as well as the POD reduced-order model were carried out to demonstrate the efficiency and the accuracy of the reduced-order model for solving the PNS equations compared with the full PNS model. Different inflow conditions and different selections of snapshots were experimented to test the POD reduction technique. The efficiency of the  $H_1$  norm POD calibration is illustrated for the PNS model with increasingly higher Reynolds numbers, along with the optimal dissipation coefficient derivation, yielding the best root mean square error and correlation coefficient between the full and reduced-order PNS models. Copyright © 2011 John Wiley & Sons, Ltd.

Received 21 July 2010; Revised 6 March 2011; Accepted 12 April 2011

KEY WORDS: parabolized Navier–Stokes (PNS); proper orthogonal decomposition (POD);  $H_1$  norm POD calibration; correlation coefficient; optimal dissipation coefficient; high Reynolds number

### 1. INTRODUCTION

For steady two-dimensional or three-dimensional flow, the complete Navier–Stokes equations can be simplified by eliminating some specific terms to provide detailed flow descriptions for large Reynolds number flows. If second-order viscous terms are eliminated and only convection and pressure gradient terms are retained, we can obtain the inviscid equations (Euler equation). If only the streamwise second-order viscous terms (i.e. in the  $x$  direction along the surface, downstream direction) are eliminated, we can obtain the so-called parabolized Navier–Stokes (PNS) equations.

The PNS equations are mathematically a set of mixed hyperbolic–parabolic equations along the assumed local streamwise flow direction, which can be used to predict complex three-dimensional steady, supersonic, viscous flow fields in an efficient manner. These types of equations satisfy certain conditions based on the coefficients of the terms in the equations and also accepts one real solution in the streamwise direction. The efficiency of the PNS equations is achieved because of the fact that the equations can be solved using a space-marching finite difference technique as opposed to the time-marching technique, which is normally employed for the complete Navier–Stokes equations. In these simplified equations, just like in the boundary layer equations, one can obtain the

\*Correspondence to: I. M. Navon, Department of Scientific Computing, Florida State University, Tallahassee, FL 32306-4120, USA.

†E-mail: inavon@fsu.edu

solution by marching in the streamwise direction (i.e. the  $x$  direction) from some known initial location. This is possible because the streamwise momentum equation (i.e. the  $x$ -momentum equation) has only first-order terms in the streamwise direction with the second-order viscous terms having been already eliminated. The PNS equations can propagate the information only in the downstream direction; thus, they are not suitable for general flow situations, especially flows with separation.

Proper orthogonal decomposition (POD), also known as Karhunen–Loeve expansions in signal analysis and pattern recognition [1], or principal component analysis in statistics [2], or the method of empirical orthogonal functions in geophysical fluid dynamics [3] or meteorology [4], is a model reduction technique offering adequate approximation for representing fluid flows with a reduced number of degrees of freedom, that is, with lower-dimensional models [5–7]. The POD method changes the complex partial differential equations to a set of much simpler ordinary differential equations of an efficiently reduced order so as to alleviate both the computational load and the memory requirements.

Because of the truncation applied in the POD reduced-order space, there is some information of the state variables missing in the POD reduced-order model. This neglected information has a very important impact on the efficiency and the stability of the POD reduced-order model for flows with high Reynolds number (e.g.  $10^3$ ) as is our case. To improve the accuracy and the long-term stability of the POD reduced-order model, Galerkin projection is insufficient and numerical stabilization is required. This is provided by an artificial dissipation that is introduced using the Sobolev  $H_1$  inner product norm to calibrate the POD method.

In the present article, we apply the POD method to derive a reduced-order model of the PNS equations and introduce an  $H_1$  norm POD calibration to solve the reduced-order model more robustly. The feasibility of the POD reduced-order model compared with the full PNS model and the efficiency of the  $H_1$  norm POD calibration in the presence of high Reynolds number are both analyzed. Because the PNS equations are already simplified Navier–Stokes equations, the POD reduced-order modeling applied to the PNS equations will yield a double benefit, namely the POD model reduction as well as the simplification of the PNS equations. To the best of our knowledge, this is a new contribution and the first application of POD reduced-order modeling to the PNS equations.

The present paper is organized as follows. Section 2 presents the specific model description of the PNS equations and the space-marching finite difference scheme with time relaxation to be used here. Section 3 provides the construction process of the POD reduced-order model, consisting of Section 3.1, where the basic theory of the POD method is provided, and Section 3.2, which illustrates the process of applying the POD method to the PNS equations to obtain the POD reduced model, which are a set of ordinary differential equations of the POD coefficients. Section 4 presents the Sobolev  $H_1$  inner product norm calibration being applied to the POD construction process in order to enhance dissipation and increase the relevance of small-scale information in the POD reduced-order model for a high Reynolds number case. In Section 5, we present numerical results, which demonstrate the efficiency of the reduced-order method for solving the PNS equations compared with the full PNS model, using the POD reduced-order model. Different inflow conditions and different numbers of snapshots are experimented to test the POD reduction technique. The efficiency of the Sobolev  $H_1$  norm POD calibration in the presence of increasingly higher Reynolds numbers is also demonstrated using a numerically derived optimal dissipation coefficient. In Section 6, the summary and conclusions are provided, including a discussion related to future research work.

## 2. PNS MODEL DESCRIPTION

For the PNS equations, the streamwise momentum equation (i.e. the  $x$ -momentum equation) has only first-order terms in the streamwise direction with the second-order viscous terms having been already eliminated. The PNS equations can propagate the information only in the downstream direction; thus, they are not suitable for general flow situations, especially flows with separation. However, the PNS equations have been applied successfully for a variety of two-dimensional and three-dimensional supersonic flows, even with real gas effects, such as compressible hypersonic flows and flows with upstream influences due to strong shock interactions and confined regions of reverse flow.

In this paper, the two-dimensional steady supersonic laminar flow is modeled by the PNS equations [8]. This model is valid if the flow is supersonic along the  $x$  coordinate, and the second-order viscous effects along this direction are negligible, a fact that allows a rapid decrease in the computational time required to complete the calculation [9]. The following equations describe an under-expanded jet (Figure 1) in this flow.

$$\begin{cases} \frac{\partial(\rho u)}{\partial x} + \frac{\partial(\rho v)}{\partial y} = 0, \\ u \frac{\partial u}{\partial x} + v \frac{\partial u}{\partial y} + \frac{1}{\rho} \frac{\partial p}{\partial x} = \frac{1}{Re\rho} \frac{\partial^2 u}{\partial y^2}, \\ u \frac{\partial v}{\partial x} + v \frac{\partial v}{\partial y} + \frac{1}{\rho} \frac{\partial p}{\partial y} = \frac{4}{3Re\rho} \frac{\partial^2 v}{\partial y^2}, \\ u \frac{\partial e}{\partial x} + v \frac{\partial e}{\partial y} + (\kappa - 1)e \left( \frac{\partial u}{\partial x} + \frac{\partial v}{\partial y} \right) = \frac{1}{\rho} \left( \frac{\kappa}{RePr} \frac{\partial^2 e}{\partial y^2} + \frac{4}{3Re} \left( \frac{\partial u}{\partial y} \right)^2 \right), \\ p = \rho RT, e = C_v T = \frac{R}{(\kappa - 1)T}, \quad (x, y) \in \Omega = (0 < x < x_{\max}, 0 < y < 1), \end{cases} \quad (2.1)$$

where  $u$  and  $v$  represent the velocity components along the  $x$  and  $y$  directions, respectively,  $\rho$  represents the flow density,  $p$  the pressure,  $e$  the specific energy,  $R$  the gas constant,  $T$  the temperature,  $C_v$  the specific volume heat capacity, and  $\kappa$  the specific heat ratio. Besides,  $Re = (\rho_{\infty} u_{\infty} y_{\max}) / (\mu_{\infty})$  is the Reynolds number, where  $\infty$  indicates the inflow boundary parameter,  $y_{\max}$  is the length of the flow field in the  $y$  direction, and  $\mu$  represents viscosity.

The following conditions are used for the inflow boundary (see A in Figure 1):

$$\rho(0, y) = \rho_{\infty}(y), \quad u(0, y) = u_{\infty}(y), \quad v(0, y) = v_{\infty}(y), \quad e(0, y) = e_{\infty}(y), \quad (2.2)$$

where  $\rho_{\infty}(y)$ ,  $u_{\infty}(y)$ ,  $v_{\infty}(y)$ , and  $e_{\infty}(y)$  are all given functions.

The lateral boundary (see B and C in Figure 1) conditions are prescribed as follows:

$$\frac{\partial \rho(x, y)}{\partial y} \Big|_{y=0} = 0, \quad \frac{\partial u(x, y)}{\partial y} \Big|_{y=0} = 0, \quad \frac{\partial v(x, y)}{\partial y} \Big|_{y=0} = 0, \quad \frac{\partial e(x, y)}{\partial y} \Big|_{y=0} = 0, \quad (2.3)$$

$$\frac{\partial \rho(x, y)}{\partial y} \Big|_{y=1} = 0, \quad \frac{\partial u(x, y)}{\partial y} \Big|_{y=1} = 0, \quad \frac{\partial v(x, y)}{\partial y} \Big|_{y=1} = 0, \quad \frac{\partial e(x, y)}{\partial y} \Big|_{y=1} = 0. \quad (2.4)$$

A space-marching finite difference discretization [10] is employed in Equations (2.5)–(2.8) to derive the solution of this problem. The finite difference discretization is of second-order accuracy in the  $y$  direction and of first order in the  $x$  direction. At every step along the  $x$  coordinate, the flow parameters are calculated from the initial inflow location in an iterative manner assuming the form of time relaxation.

Continuity equation:

$$\frac{\rho_{i,j}^{n+1} - \rho_{i,j}^n}{\tau} + u_{i,j}^n \frac{\rho_{i,j}^n - \rho_{i-1,j}^n}{\Delta x} + v_{i,j}^n \frac{\rho_{i,j+1}^{n+1} - \rho_{i,j-1}^{n+1}}{2\Delta y} + \rho_{i,j}^n \left( \frac{u_{i,j}^n - u_{i-1,j}^n}{\Delta x} + \frac{v_{i,j}^n - v_{i,j-1}^n}{\Delta y} \right) = 0 \quad (2.5)$$

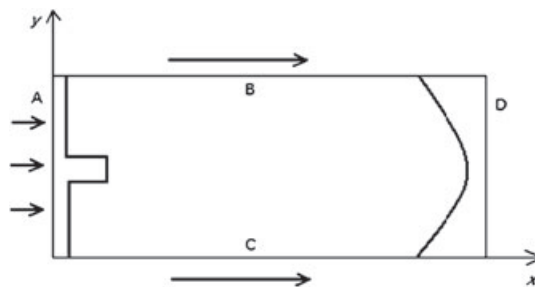


Figure 1. Flow region. A, inflow boundary; B and C, lateral boundaries; D, outflow boundary (measurement).

Momentum equations:

$$\begin{aligned} & \frac{u_{i,j}^{n+1} - u_{i,j}^n}{\tau} + u_{i,j}^n \frac{u_{i,j}^n - u_{i-1,j}^n}{\Delta x} + v_{i,j}^n \frac{u_{i,j+1}^{n+1} - u_{i,j-1}^{n+1}}{2\Delta y} + \frac{p_{i,j}^n - p_{i-1,j}^n}{\Delta x \rho_{i,j}^n} \\ & - \frac{1}{Re\rho_{i,j}^n} \frac{u_{i,j+1}^{n+1} - 2u_{i,j}^{n+1} + u_{i,j-1}^{n+1}}{\Delta y^2} = 0 \end{aligned} \tag{2.6}$$

$$\begin{aligned} & \frac{v_{i,j}^{n+1} - v_{i,j}^n}{\tau} + u_{i,j}^n \frac{v_{i,j}^n - v_{i-1,j}^n}{\Delta x} + v_{i,j}^n \frac{v_{i,j+1}^{n+1} - v_{i,j-1}^{n+1}}{2\Delta y} + \frac{p_{i,j}^n - p_{i,j-1}^n}{\Delta y \rho_{i,j}^n} \\ & - \frac{4}{3Re\rho_{i,j}^n} \frac{v_{i,j+1}^{n+1} - 2v_{i,j}^{n+1} + v_{i,j-1}^{n+1}}{\Delta y^2} = 0 \end{aligned} \tag{2.7}$$

Energy equation:

$$\begin{aligned} & \frac{e_{i,j}^{n+1} - e_{i,j}^n}{\tau} + u_{i,j}^n \frac{e_{i,j}^n - e_{i-1,j}^n}{\Delta x} + v_{i,j}^n \frac{e_{i,j+1}^{n+1} - e_{i,j-1}^{n+1}}{2\Delta y} + (\kappa - 1)e_{i,j}^n \left( \frac{u_{i,j}^n - u_{i-1,j}^n}{\Delta x} + \frac{v_{i,j}^n - v_{i,j-1}^n}{\Delta y} \right) \\ & - \frac{1}{\rho_{i,j}^n} \left( \frac{\kappa}{RePr} \frac{e_{i,j+1}^{n+1} - 2e_{i,j}^{n+1} + e_{i,j-1}^{n+1}}{\Delta y^2} + \frac{4}{3Re} \left( \frac{u_{i,j}^n - u_{i,j-1}^n}{\Delta y} \right)^2 \right) = 0 \end{aligned} \tag{2.8}$$

where  $i$  and  $j$  denote the node index along the  $x$  and  $y$  coordinates, respectively,  $n$  is the number of time iterations, and  $\tau$  is the relaxation factor.

### 3. POD REDUCED-ORDER MODEL OF PNS

Proper orthogonal decomposition is a technique that provides a useful tool for efficiently approximating a large amount of data and representing fluid flows with a reduced number of degrees of freedom. It is also very efficient in the sense that it can capture the greatest possible energy in a reduced space [11]. We apply this method to obtain a reduced-order model of the above PNS equations and expect it to yield a decrease in both the computational load and the CPU time, which lays the foundation for proceeding to the next stage, that is, the POD 4-D VAR [6, 11] inverse problem [12–14].

#### 3.1. Proper orthogonal decomposition

Let  $V$  represent the model variables (e.g.  $u$ ,  $v$ ,  $e$ , and  $p$ ). The ensemble of snapshots sampled at designated time steps  $\{V^l\}_{l=1}^L = \{V_i^l\}_{i=1}^L$  ( $1 \leq i \leq M$ ) ( $L \leq N$ ) can be expressed as the following  $M \times L$  matrix  $A_V$ , where  $M$  is the number of nodes,  $N$  is the number of time steps, and  $L$  is the number of snapshots.

$$A_V = \begin{pmatrix} V_1^1 & V_1^2 & \cdots & V_1^L \\ V_2^1 & V_2^2 & \cdots & V_2^L \\ \vdots & \vdots & \vdots & \vdots \\ V_M^1 & V_M^2 & \cdots & V_M^L \end{pmatrix} \tag{3.1}$$

The average of the ensemble of snapshots  $\{\bar{V}_i\}_{i=1}^M$  is defined as

$$\bar{V}_i = \frac{1}{L} \sum_{l=1}^L V_i^l, \quad 1 \leq i \leq M, \tag{3.2}$$

$$\hat{V}_i^l = V_i^l - \bar{V}_i, \quad 1 \leq i \leq M, 1 \leq l \leq L, \tag{3.3}$$

which constructs an  $M \times L$  matrix  $A = \{\widehat{V}^i\}_{i=1}^L$ .

The essence of the POD method is to find a set of orthogonal basis functions  $\{\phi_i\} (i = 1, \dots, L)$  to maximize the inner product defined as

$$\frac{1}{L} \sum_{i=1}^L |\langle \widehat{V}^i, \phi_i \rangle_{L^2}|^2 \quad (3.4)$$

subject to the normalized orthogonality conditions

$$\begin{aligned} \langle \phi_i, \phi_j \rangle_{L^2} &= 1, & i &= j \\ \langle \phi_i, \phi_j \rangle_{L^2} &= 0, & i &\neq j, \end{aligned} \quad (3.5)$$

where  $i, j = 1, 2, \dots, L$  and the inner product is defined in the  $L^2$  space as  $\langle f, g \rangle_{L^2} = \int_{\Omega} fg \, d\Omega$  in which  $f$  and  $g$  are two real functions defined on the measure space  $\Omega$ .

With the use of the  $L^2$  inner product, the above optimization problem becomes

$$\max_{\phi_i \in L^2} \frac{1}{L} \sum_{i=1}^L |\langle \widehat{V}^i, \phi_i \rangle_{L^2}|^2 = \max_{\phi_i \in L^2} \frac{1}{L} \sum_{i=1}^L \int_{\Omega} \widehat{V}^i \phi_i \, d\Omega. \quad (3.6)$$

Because the basis functions can be represented as the linear combination of the solution snapshots,

$$\phi = \sum_{i=1}^L a_i \widehat{V}^i, \quad (3.7)$$

the optimization problem changes to the following eigenvalue problem:

$$Cx = \lambda x, \quad (3.8)$$

where

$$C = \{c_{i,j}\}_{i,j=1}^M = \left\{ \int_{\Omega} (\widehat{V}^i)^T \widehat{V}^j \, d\Omega \right\}_{i,j=1}^M = AA^T. \quad (3.9)$$

In order to solve the above eigenvalue problem, we employed the singular value decomposition method to obtain an optimal representation for  $A$  and the eigenvectors for  $C$  [5, 15], which is an important tool to construct the optimal basis of reduced-order approximation.

By neglecting the modes corresponding to the smallest singular eigenvalues, we can estimate the energy captured by the first  $m$  POD basis functions using [16, 17]

$$I(m) = \frac{\sum_{i=1}^m \lambda_i}{\sum_{i=1}^L \lambda_i}, \quad (3.10)$$

where  $I(m)$  represents the ratio of energy captured in the first  $m$  modes to the total energy.

Hence, the state variable can be represented by the linear combination of the retained POD basis functions as follows:

$$V(x, y) = \bar{V} + \sum_{i=1}^m \alpha_i(x) \phi_i(y), \quad (3.11)$$

where  $\alpha_i(x)$  ( $i = 1, \dots, m$ ) are the POD coefficients corresponding to every POD basis function. Note that the  $x$  direction is taken as time and the  $y$  direction is taken as space in the PNS model.

3.2. *POD reduced model*

In the following, we use the POD basis functions derived above to develop a reduced-order PNS model, in which the marching direction  $x$  is taken to represent the time evolution. The flow variables are modeled as

$$\rho(x, y) = \bar{\rho} + \sum_{i=1}^m \alpha_i^\rho(x) \phi_i^\rho(y), \tag{3.12}$$

$$u(x, y) = \bar{u} + \sum_{i=1}^m \alpha_i^u(x) \phi_i^u(y), \tag{3.13}$$

$$v(x, y) = \bar{v} + \sum_{i=1}^m \alpha_i^v(x) \phi_i^v(y), \tag{3.14}$$

$$e(x, y) = \bar{e} + \sum_{i=1}^m \alpha_i^e(x) \phi_i^e(y), \tag{3.15}$$

where  $\bar{\rho}$ ,  $\bar{u}$ ,  $\bar{v}$ , and  $\bar{e}$  represent the mean of the ensemble of snapshots for the variables of the PNS equations;  $\alpha_i^\rho$ ,  $\alpha_i^u$ ,  $\alpha_i^v$ , and  $\alpha_i^e$ , ( $1 \leq i \leq m$ ) are coefficients related to the POD basis functions for the state variables to be determined; and  $\alpha_i(0)$  are the known coefficients at the inflow location defined by the following:

$$\rho(0, y) = \bar{\rho} + \sum_{i=1}^m \alpha_i^\rho(0) \phi_i^\rho(y), \tag{3.16}$$

$$u(0, y) = \bar{u} + \sum_{i=1}^m \alpha_i^u(0) \phi_i^u(y), \tag{3.17}$$

$$v(0, y) = \bar{v} + \sum_{i=1}^m \alpha_i^v(0) \phi_i^v(y), \tag{3.18}$$

$$e(0, y) = \bar{e} + \sum_{i=1}^m \alpha_i^e(0) \phi_i^e(y). \tag{3.19}$$

After substituting Equations (3.8)–(3.11) into the parabolic Navier–Stokes equations of Equation (2.1) and then taking the inner product with the POD basis for each flow variable, we obtain a set of ordinary differential equations of the POD coefficients  $\alpha_i^\rho$ ,  $\alpha_i^u$ ,  $\alpha_i^v$ , and  $\alpha_i^e$ .

Thus, we can obtain the POD reduced-order model of size  $4 \times m \times M$  ( $m \ll L \ll N$ ), which can be compared with the full PNS of size  $4 \times N \times M$ .

4. FORMULATION OF POD CALIBRATION USING SOBOLEV  $H_1$  NORM

High Reynolds number flows exhibit dynamics on a wide range of scales. The POD reduced-order model derived from the finite difference discretization is not sufficiently accurate in reproducing the dynamics of high Reynolds number flows because the truncation applied in the POD subspace neglects the low-energy modes that represent some important but fine-scale information of the fluid flow [18]. The neglected POD modes corresponding to small-scale structures introduce dissipation errors in the model because usually dissipation of energy occurs mainly on the level of scales that are

unresolved in the discretization [19]. Consequently, the dynamic system may lose its long-term stability. To ensure that the smaller scales are retained in the POD model and enhance dissipation, we introduced an artificial dissipation by using a Sobolev  $H_1$  inner product norm to calibrate the POD method, that is, the derivatives of the snapshots and those of the basis functions are both included in the formulation of the optimization problem [20].

Thus, the optimization problem in this calibrated POD process consists in seeking the POD basis functions  $\phi_i, i = 1, \dots, L$  to maximize

$$\frac{1}{L} \sum_{i=1}^L (\langle A, \phi_i \rangle)^2 = \frac{1}{L} \sum_{i=1}^L \int_{\Omega} A \phi_i d\Omega + \epsilon \int_{\Omega} \nabla A \nabla \phi_i d\Omega \tag{4.1}$$

subject to

$$\begin{aligned} \langle \phi_i, \phi_j \rangle_{H_1} &= 1, & i = j \\ \langle \phi_i, \phi_j \rangle_{H_1} &= 0, & i \neq j, \end{aligned} \tag{4.2}$$

where  $i, j = 1, \dots, L$ .

The corresponding eigenvalue problem becomes

$$Cx = \lambda x, \tag{4.3}$$

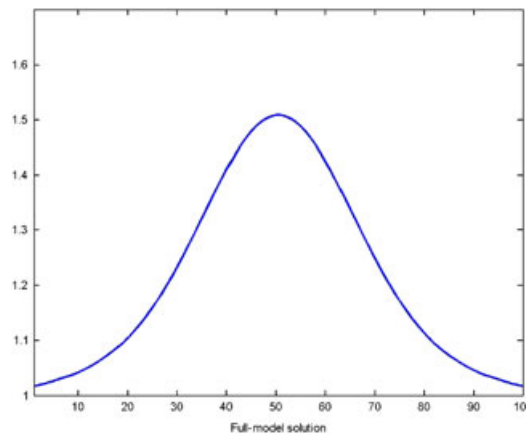


Figure 2. The initial condition for the specific energy  $e$  at the inflow boundary  $A$  (see Figure 1).

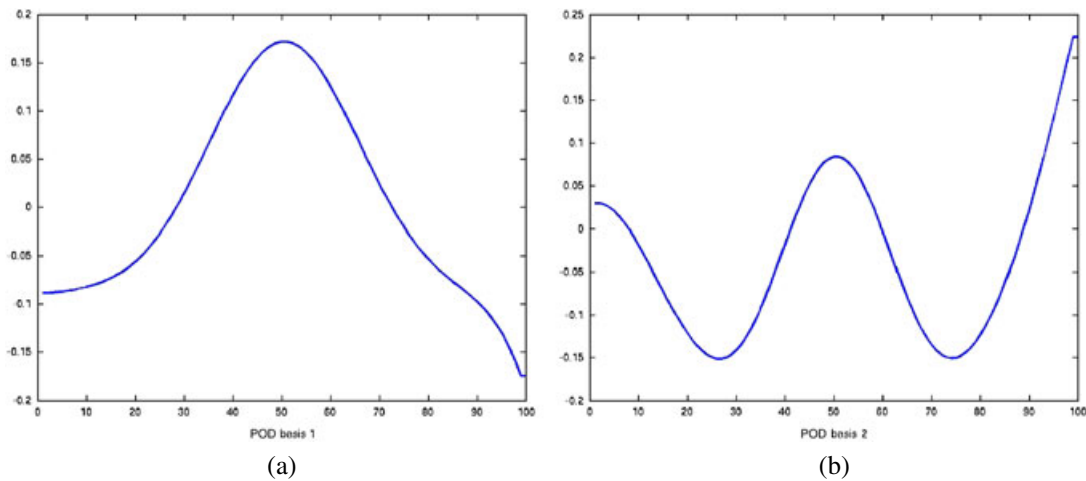


Figure 3. The (a) first and (b) second POD basis functions of the specific energy  $e$ .

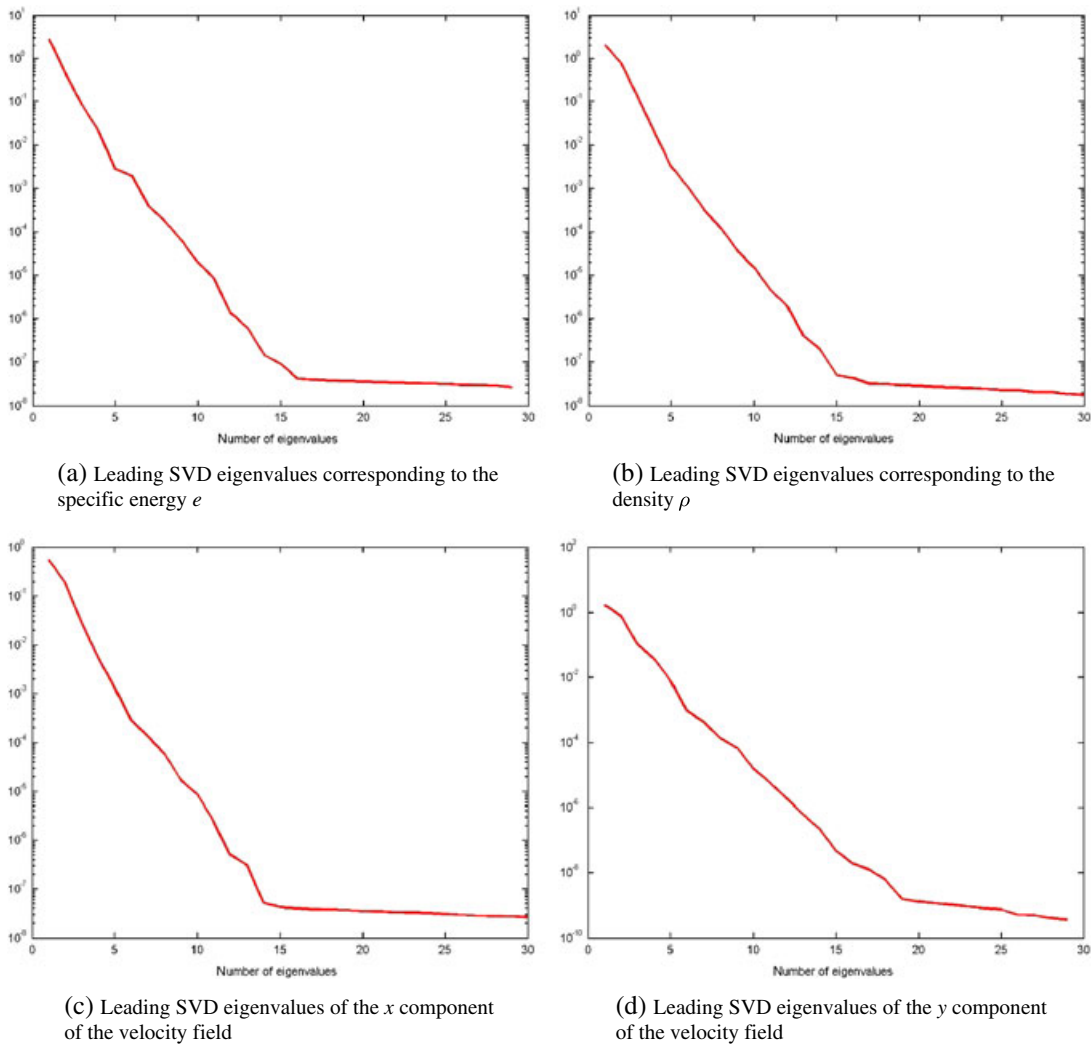


Figure 4. (a–d) Singular value decomposition (SVD) eigenvalues in a decreasing order of magnitude ( $Re = 1000$ ).

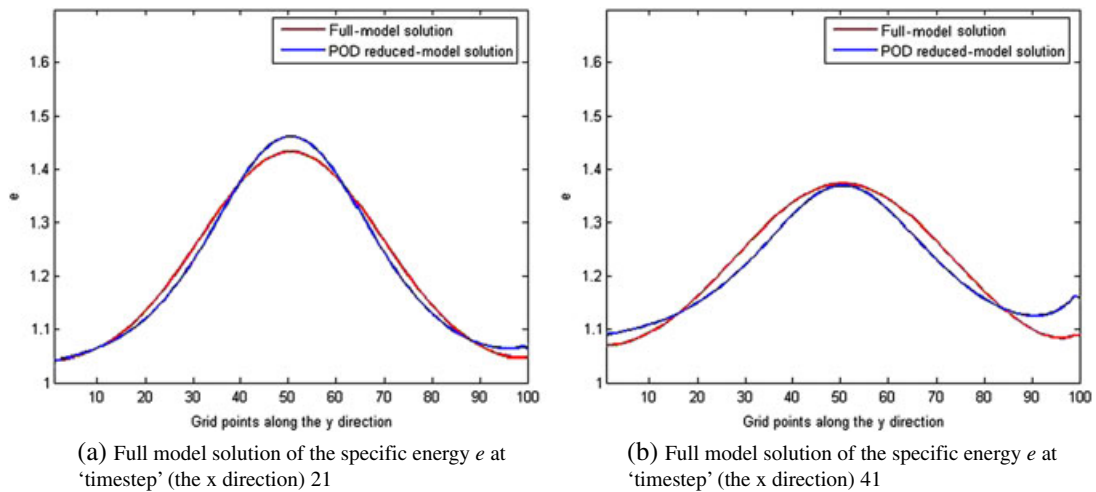


Figure 5. (a) Full-model solution and (b) POD reduced-order model solution of the PNS equations ( $Re = 1000$ ).

where

$$C = \{c_{i,j}\}_{i,j=1}^M = \left\{ \int_{\Omega} (\widehat{V}^i)^T \widehat{V}^j d\Omega + \epsilon \left( \int_{\Omega} \nabla(\widehat{V}^i)^T \nabla \widehat{V}^j d\Omega \right) \right\}_{i,j=1}^M = AA^T + \nabla A \nabla A^T, \quad (4.4)$$

where  $\epsilon$  is the dissipation coefficient whose value can be guessed to be proportional to  $T/Re$  because of dimensional analysis considerations, where  $T$  is some appropriate timescale [20].

## 5. NUMERICAL RESULTS

In this section, the flow field is computed by marching along the  $x$  coordinate, which represents the time evolution from  $x = 0$  to  $x = x_{\max}$ . The computational grid contains 50–100 points in the marching direction (the  $x$  direction) and 100 points in the transversal direction (the  $y$  direction). We experimented with different Reynolds numbers and different numbers of snapshots to test the performance of the POD method.

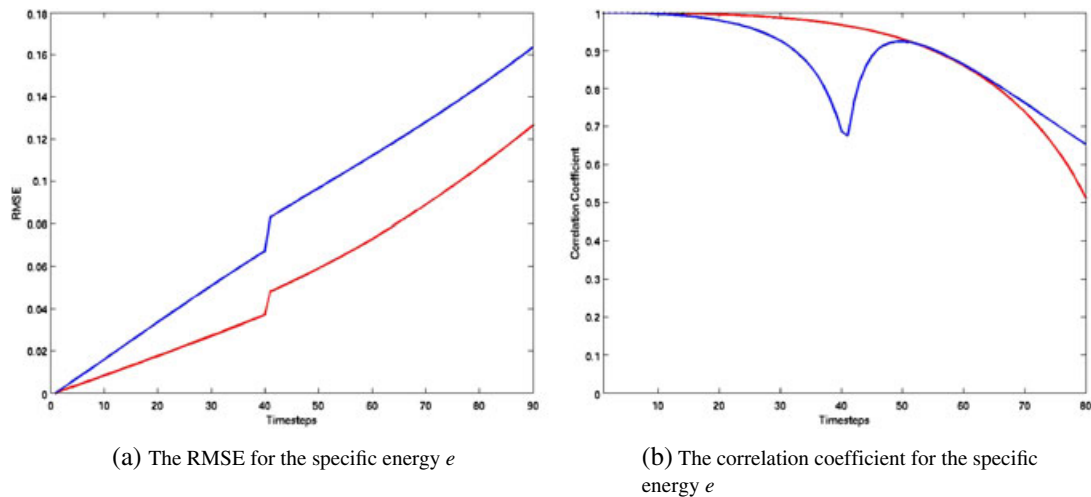


Figure 6. (a, b) Impact of the number of snapshots on the POD model reduction (blue: 100 snapshots, red: 200 snapshots) ( $Re = 1000$ ). RMSE, root mean square error.

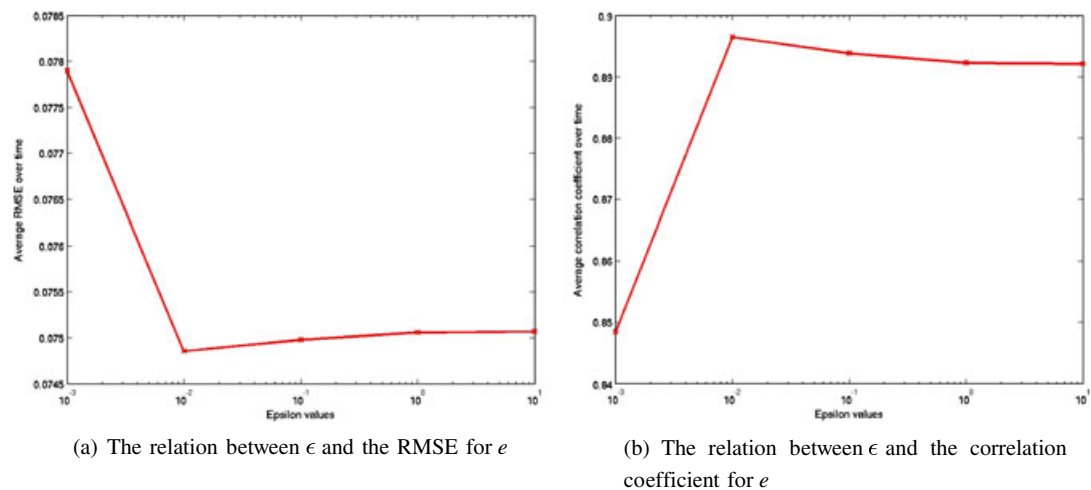


Figure 7. The variation of the (a) root mean square error (RMSE) and the (b) correlation coefficient as a function of different values of the dissipation coefficient  $\epsilon$  ( $Re = 1000$ ).

5.1. Numerical results of the POD reduced-order model

We chose the Reynolds number as  $Re = 10^3$  in this test. Let the length of the flow field in the  $x$  direction be normalized to 1. Figure 2 shows the initial specific energy  $e$  of the flow at the inflow boundary A ( $x = 0$ , Figure 1), which was obtained using the logistic function. Figure 3 presents the first and second POD basis functions for the specific energy  $e$  using 100 snapshots in which we can observe that the first POD basis function captures the dominant characteristics of the specific energy  $e$ . Figure 4 shows the first 30 leading eigenvalues of the singular value decomposition for the POD model reduction of the PNS equations corresponding to the different state variables in a decreasing order of magnitude, and one can observe that the first six leading POD eigenvalues account for more than 99.9% of the total energy (see Equation (3.14)).

Figure 5 shows the full-model solutions compared with the corresponding POD reduced-order solutions for the specific energy  $e$  at the 21st and 41st  $x$ -direction nodes.

In the present paper, the root mean square error (RMSE) and the correlation coefficient (COR) between the full PNS and POD models are defined as

$$RMSE^l = \sqrt{\frac{\sum_{i=1}^M (V_i^l - V_{0,i}^l)^2}{M}}, \quad l = 1, \dots, L \tag{5.5}$$

and

$$COR^l = \frac{\sum_{i=1}^M (V_i^l - \bar{V}^l)(V_{0,i}^l - \bar{V}_0^l)}{\sqrt{\sum_{i=1}^M (V_i^l - \bar{V}^l)^2} \sqrt{\sum_{i=1}^M (V_{0,i}^l - \bar{V}_0^l)^2}}, \quad l = 1, \dots, L, \tag{5.6}$$

where  $V_i^l$  and  $V_{0,i}^l$  are vectors containing the POD reduced-order model solution and the full-model solution of the state variables, respectively,  $\bar{V}^l$  and  $\bar{V}_0^l$  are average solutions over the  $y$  direction corresponding to the POD reduced-order model and the full PNS model, respectively,  $M$  is the number of nodes along the  $y$  direction, and  $L$  is the number of nodes in the  $x$  direction.

In order to study the impact of the number of snapshots on the POD model reduction, we doubled the number of snapshots from 100 to 200. The RMSE and the COR between the full PNS model and the POD reduced-order one derived using 100 and 200 snapshots are presented in Figure 6. We can observe that the RMSE and the COR for the specific energy  $e$  are both improved with the increase

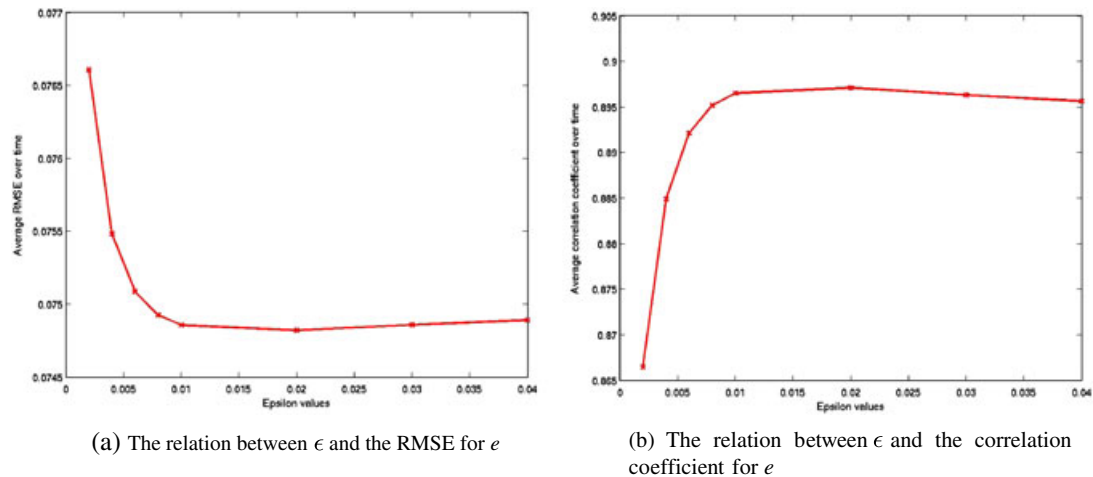


Figure 8. The variation of the (a) root mean square error (RMSE) and the (a) correlation coefficient as a function of different values of the dissipation coefficient  $\epsilon$  ( $Re = 1000$ ).

in the number of snapshots. Similar results (not shown) were obtained for the other components of the PNS flow field.

The CPU time of the POD reduced-order PNS model is approximately 1 s compared with 6 s of the full PNS model with the Core2 Duo CPU (2.80 GHz) and Windows XP operating system. Also,

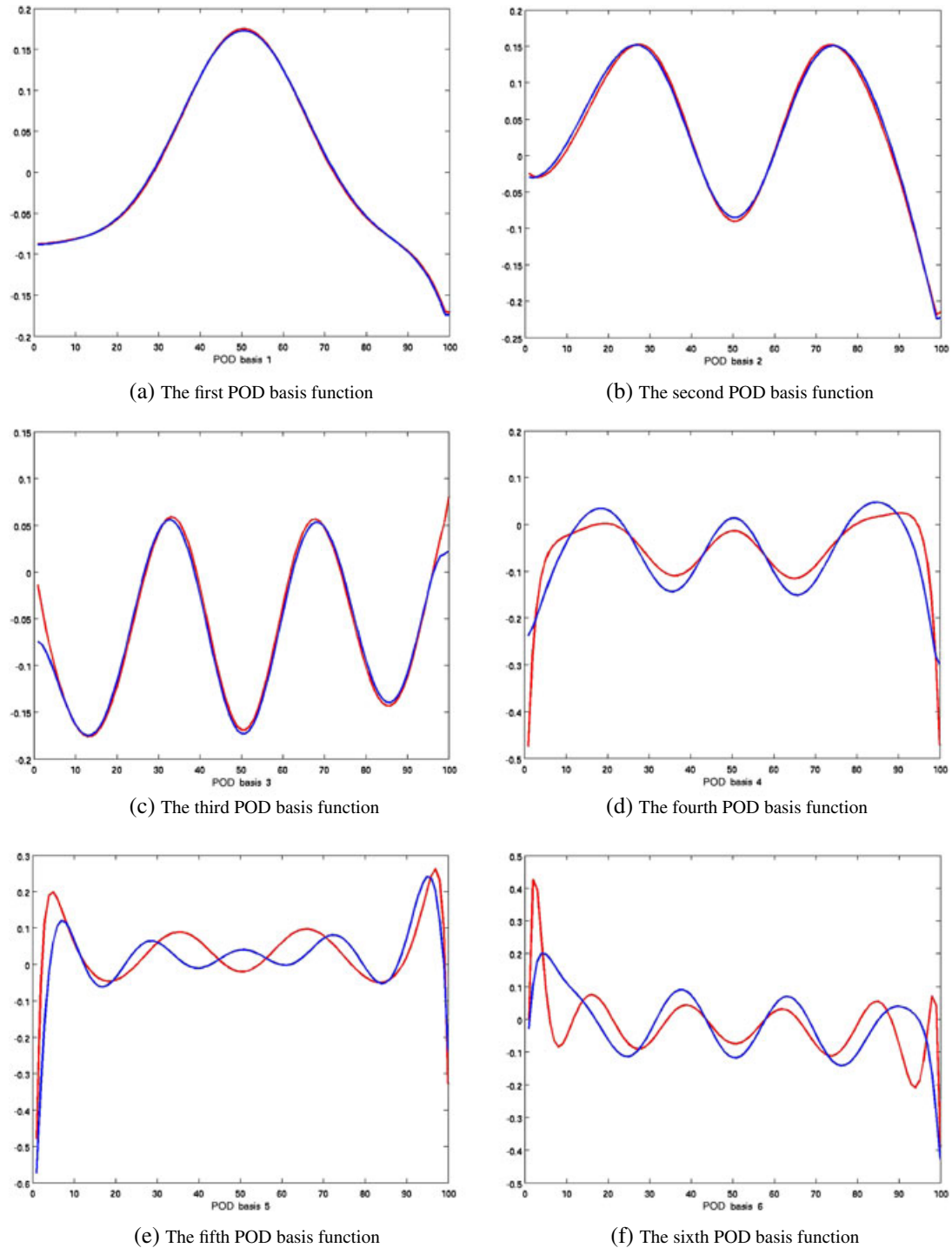


Figure 9. (a–f) The first six leading POD basis functions for  $e$  (blue: without POD calibration, red: with POD calibration using the optimal dissipation coefficient  $\epsilon = 2 \times 10^{-2}$ ) ( $Re = 1000$ ).

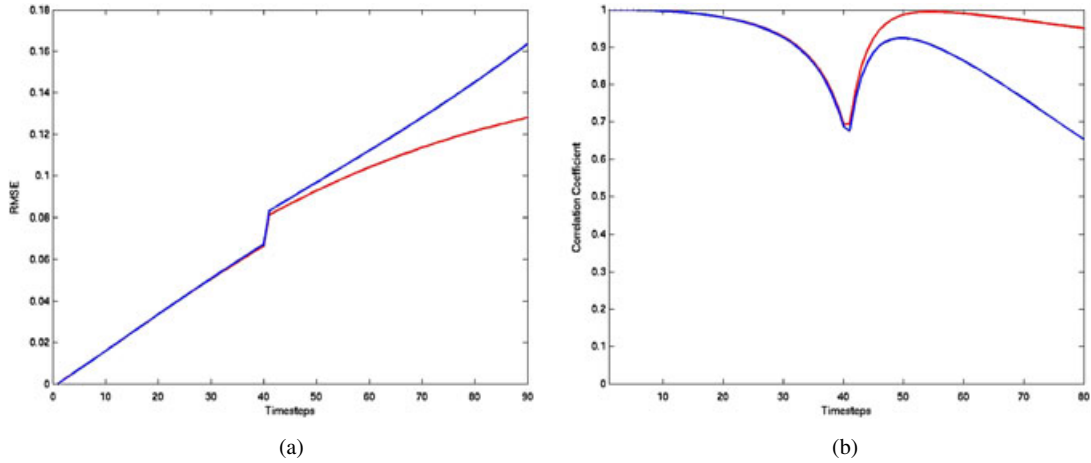


Figure 10. The (a) root mean square error (RMSE) and the (b) correlation coefficient for  $e$  between the full and POD reduced-order PNS models (blue: without POD calibration, red: with POD calibration) ( $Re = 1000$ ).

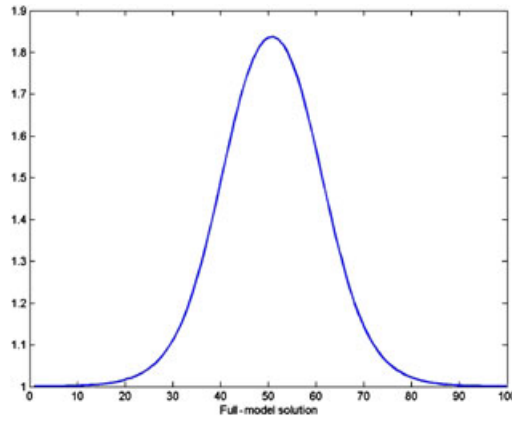


Figure 11. The initial condition for the specific energy  $e$  at the inflow boundary A (see Figure 1).

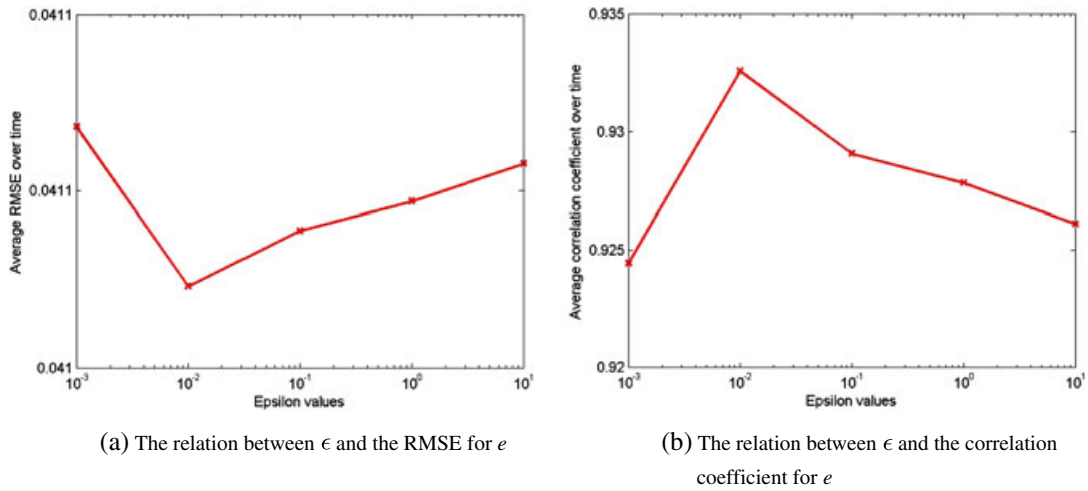


Figure 12. The variation of the (a) root mean square error (RMSE) and the (b) correlation coefficient as a function of different values of the dissipation coefficient  $\epsilon$  ( $Re = 1000$ ).

the CPU time spent on the POD basis construction process was only 0.2 s, which is very efficient compared with the simulation process.

### 5.2. Numerical results obtained with the $H_1$ norm

Because our model uses a high Reynolds number (e.g.  $Re = 10^3$ ), a calibration applied to the POD construction process [21–27] is expected to yield better numerical results. In the Sobolev  $H_1$  inner product norm POD calibration, it is very important to choose an appropriate dissipation coefficient  $\epsilon$  to improve the POD method efficiently. We tested the  $H_1$  norm POD calibration for the PNS model with  $Re = 1.0 \times 10^3$ ,  $Re = 0.6 \times 10^3$ , and  $Re = 1.2 \times 10^3$ .

**5.2.1.  $Re = 1.0 \times 10^3$ .** For the Reynolds number  $Re = 1.0 \times 10^3$ , we carried out a series of numerical experiments to determine the optimal dissipation coefficient  $\epsilon$  for the specific energy  $e$  corresponding to our test problem.

First, we chose the value of  $\epsilon$  in the interval  $10^{-3} \leq \epsilon \leq 10$  in increments of 10 to test the variation of the RMSE and the COR for the specific energy  $e$  between the full PNS model and the POD reduced-order model. The optimal value was found to be  $\epsilon = 10^{-2}$  (see Figure 7).

A more precise value of  $\epsilon$  for the specific energy  $e$  was sought in the vicinity of  $10^{-2}$  particularly. The RMSE and the COR corresponding to different values of  $\epsilon$  in the interval  $2 \times 10^{-3} \leq \epsilon \leq 4 \times 10^{-2}$  are presented in Figure 8, in which we can observe that the smallest RMSE and the largest correlation number ( $0 \leq \text{COR} \leq 1$ ) for the specific energy  $e$  between the full PNS model and the POD reduced-order one were both attained for a value of  $\epsilon = 2 \times 10^{-2}$ .

Figure 9 presents the first six leading POD basis functions with and without  $H_1$  norm POD calibration when the optimal dissipation coefficient  $\epsilon = 2 \times 10^{-2}$  was chosen.

The RMSE and the COR of the specific energy  $e$  between the full PNS model and the reduced-order PNS model using 100 snapshots with and without the Sobolev  $H_1$  norm POD calibration are presented in Figure 10. We can conclude that the POD method with the Sobolev  $H_1$  norm calibration and optimal dissipation coefficient  $\epsilon$  improves the long-term stability of the reduced-order model.

Another inflow condition at the inflow boundary A ( $x = 0$ , Figure 1) is presented in Figure 11. The variations of the RMSE and the COR for the specific energy  $e$  corresponding to different values of the dissipation coefficient  $\epsilon$  in the interval  $10^{-3} \leq \epsilon \leq 10$  and  $2 \times 10^{-2} \leq \epsilon \leq 4 \times 10^{-1}$  are presented in Figures 12 and 13, respectively. The optimal dissipation coefficient  $\epsilon$  with the smallest RMSE and the largest correlation number turned out to be  $\epsilon = 2 \times 10^{-2}$ .

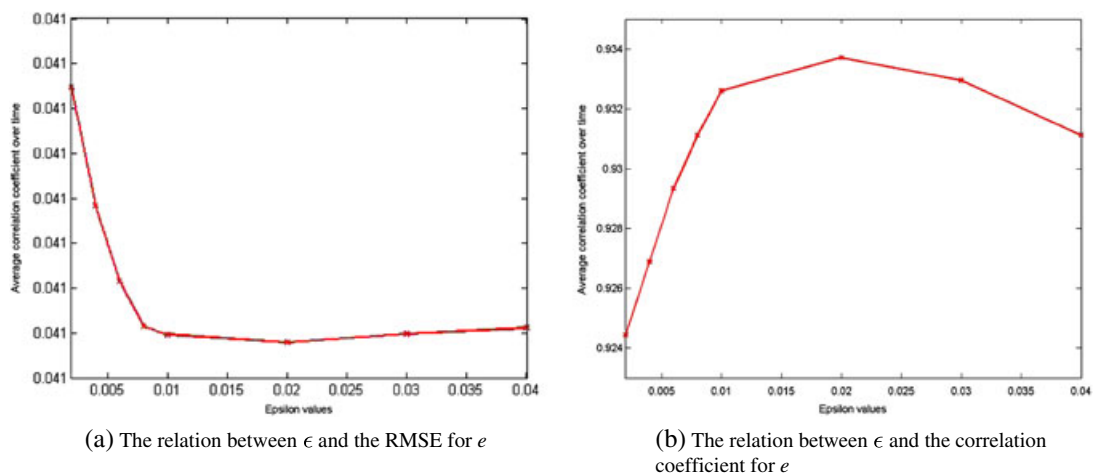


Figure 13. The variation of the (a) root mean square error (RMSE) and the (b) correlation coefficient as a function of different values of the dissipation coefficient  $\epsilon$  ( $Re = 1000$ ).

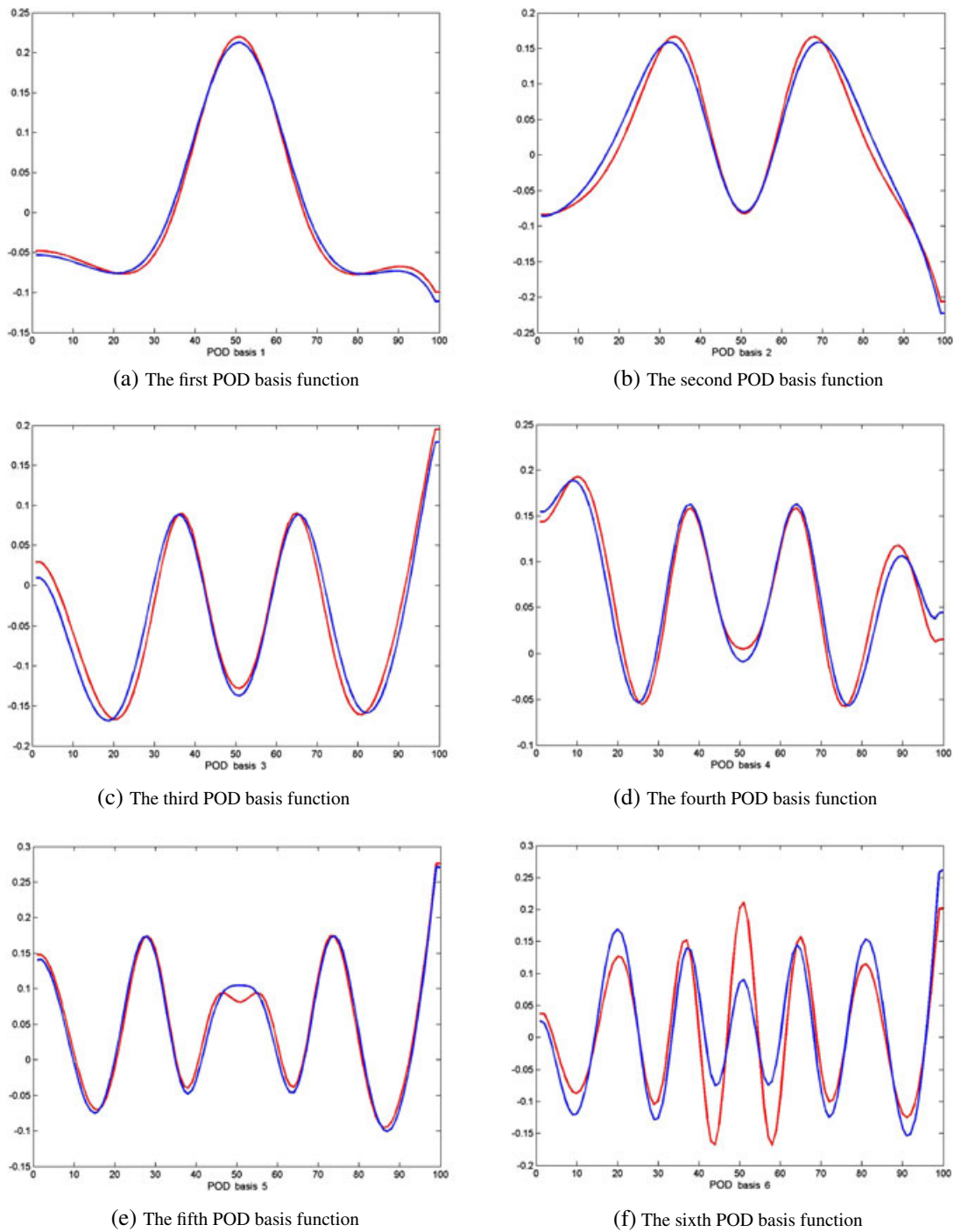


Figure 14. (a–f) The first six leading POD basis functions for  $e$  (blue: without POD calibration, red: with POD calibration using the optimal dissipation coefficient  $\epsilon = 2 \times 10^{-2}$ ) ( $Re = 1000$ ).

The first six leading POD basis functions with and without  $H_1$  norm POD calibration with the optimal dissipation coefficient  $\epsilon = 2 \times 10^{-2}$  are shown in Figure 14. The full and POD reduced model solutions for the specific energy  $e$  at the 21st and 41st time steps are presented in Figure 15.

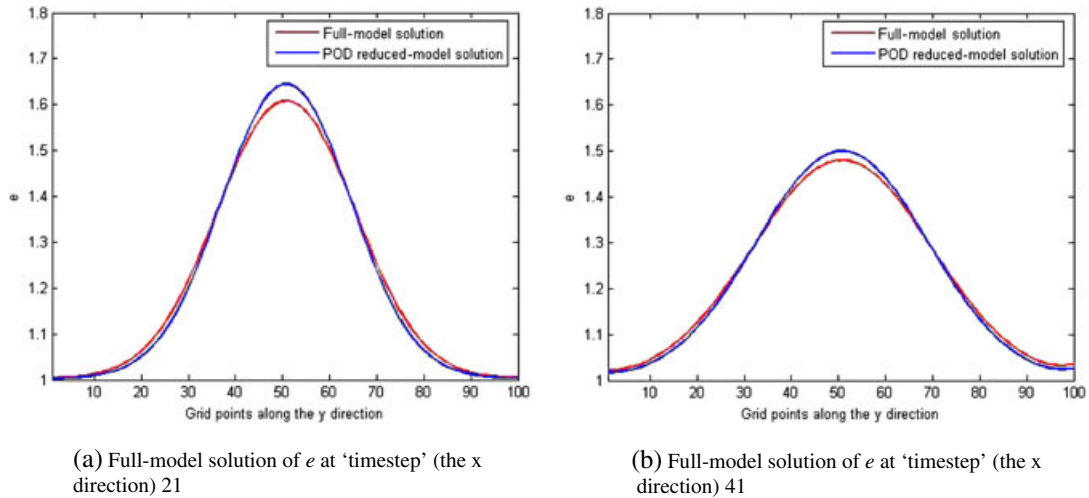


Figure 15. (a) Full-model solution and (b) POD reduced-order model solution of the PNS equations ( $Re = 1000$ ).

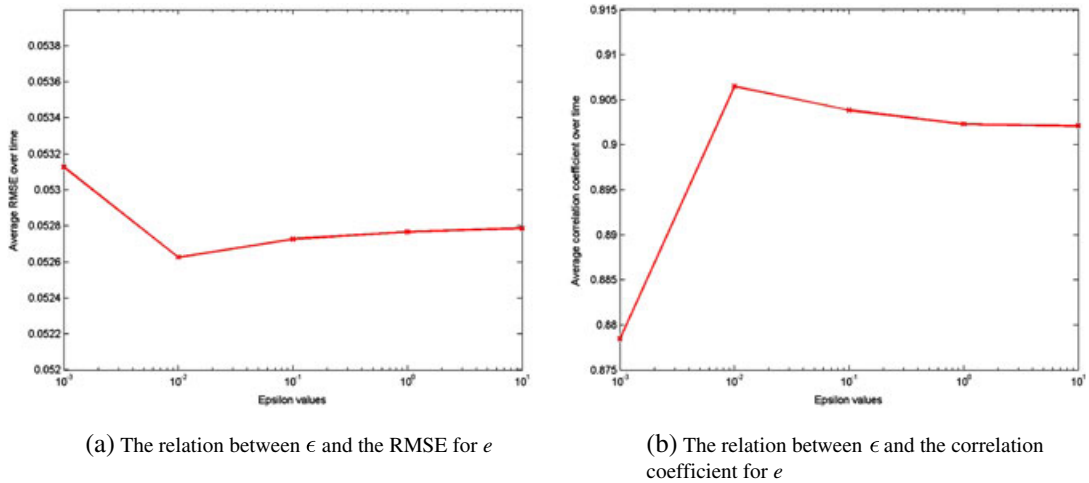


Figure 16. The variation of the (a) root mean square error (RMSE) and the (b) correlation coefficient as a function of different values of the dissipation coefficient  $\epsilon$  ( $Re = 600$ ).

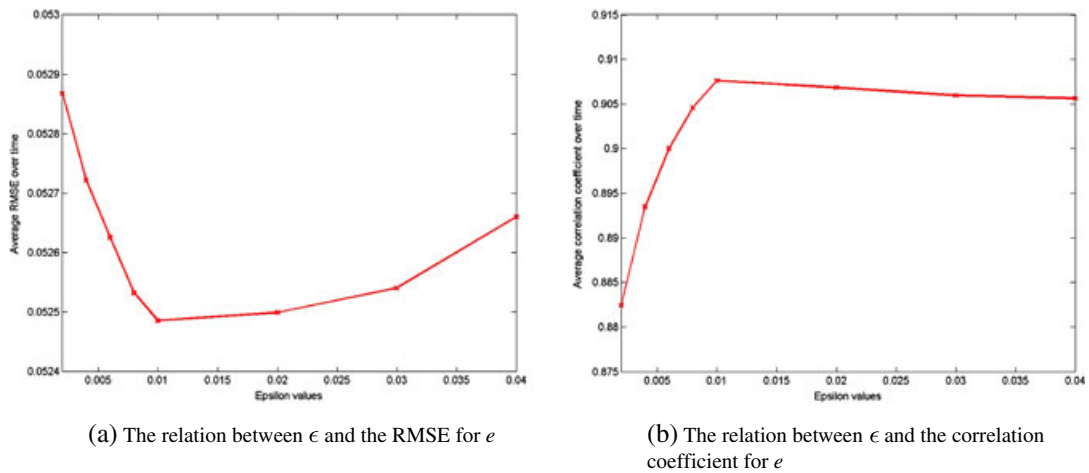


Figure 17. The variation of the (a) root mean square error (RMSE) and the (b) correlation coefficient as a function of different values of the dissipation coefficient  $\epsilon$  ( $Re = 600$ ).

5.2.2.  $Re = 0.6 \times 10^3$ . A similar series of numerical experiments to determine the optimal dissipation coefficient  $\epsilon$  for the specific energy  $e$  was carried out for the Reynolds number  $Re = 0.6 \times 10^3$ . Figures 16 and 17 show the variation of the RMSE and the COR for the specific energy  $e$  with respect to different values of  $\epsilon$  in the interval  $10^{-3} \leq \epsilon \leq 10$  and  $2 \times 10^{-3} \leq \epsilon \leq 4 \times 10^{-2}$ , respectively. The optimal value was found to be  $\epsilon = 1 \times 10^{-2}$ .

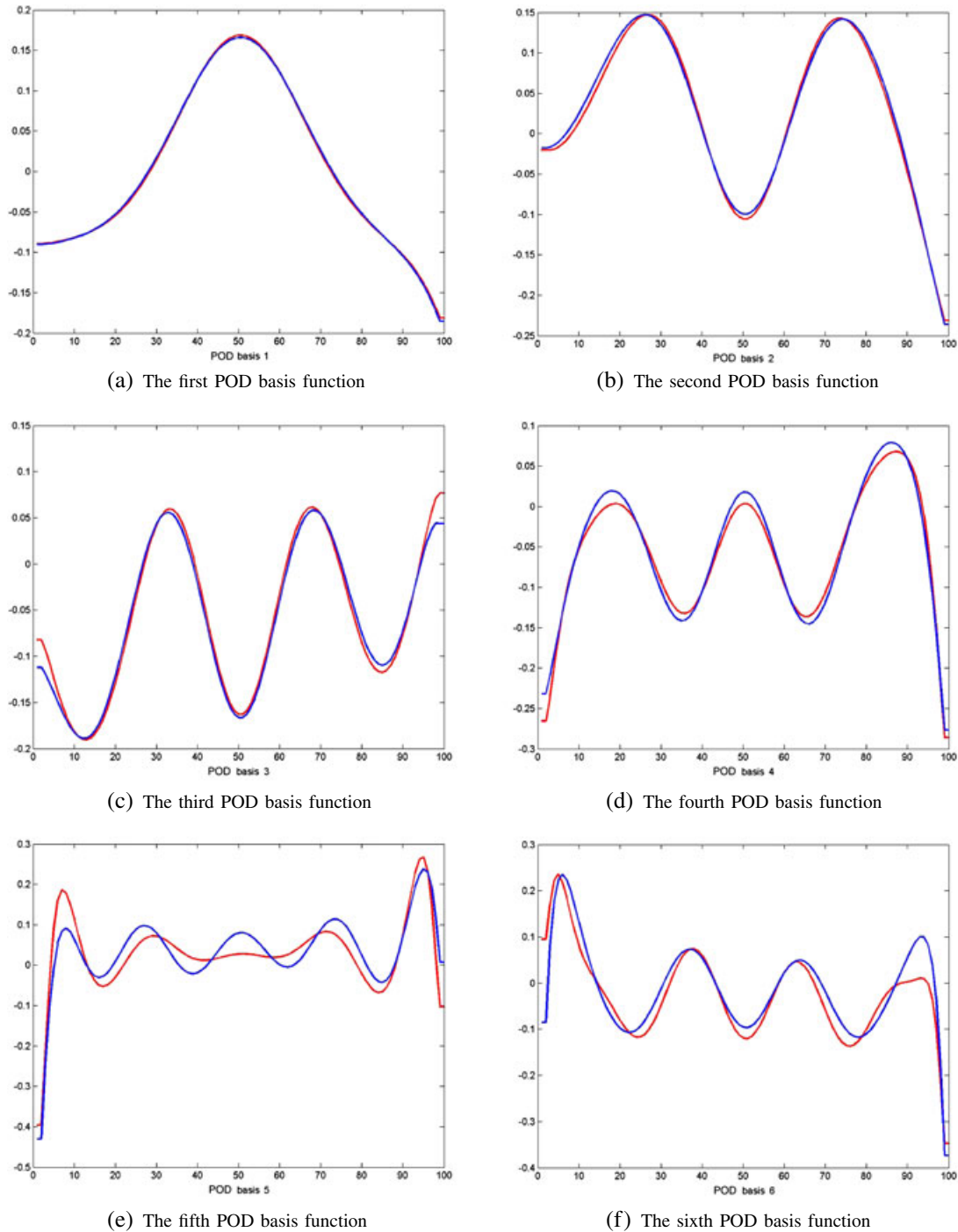


Figure 18. (a–f) The first six leading POD basis functions for  $e$  (blue: without POD calibration, red: with POD calibration using the optimal dissipation coefficient  $\epsilon = 1 \times 10^{-2}$ ) ( $Re = 600$ ).

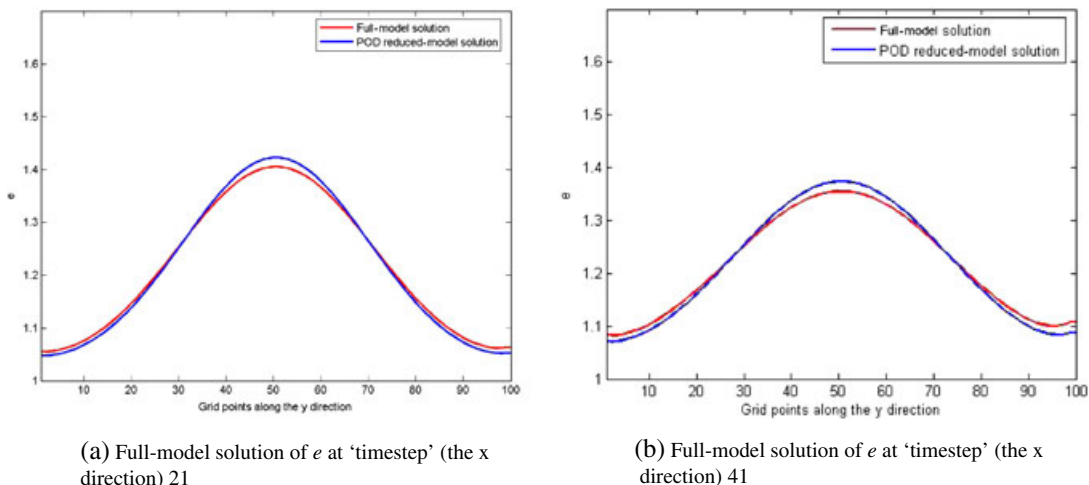


Figure 19. (a) Full-model solution and (b) POD reduced-order model solution of the PNS equations ( $Re = 600$ ).

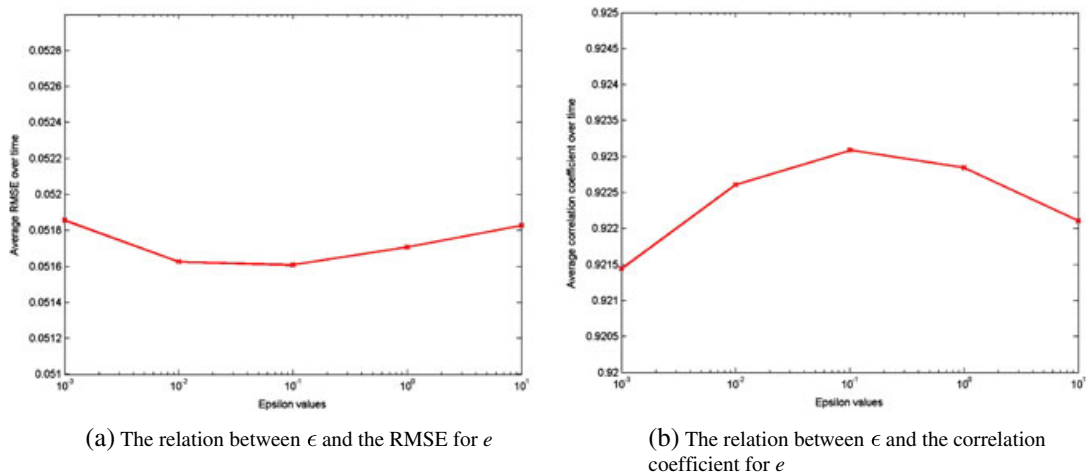


Figure 20. The variation of the (a) root mean square (RMSE) and the (b) correlation coefficient as a function of different values of the dissipation coefficient  $\epsilon$  ( $Re = 1200$ ).

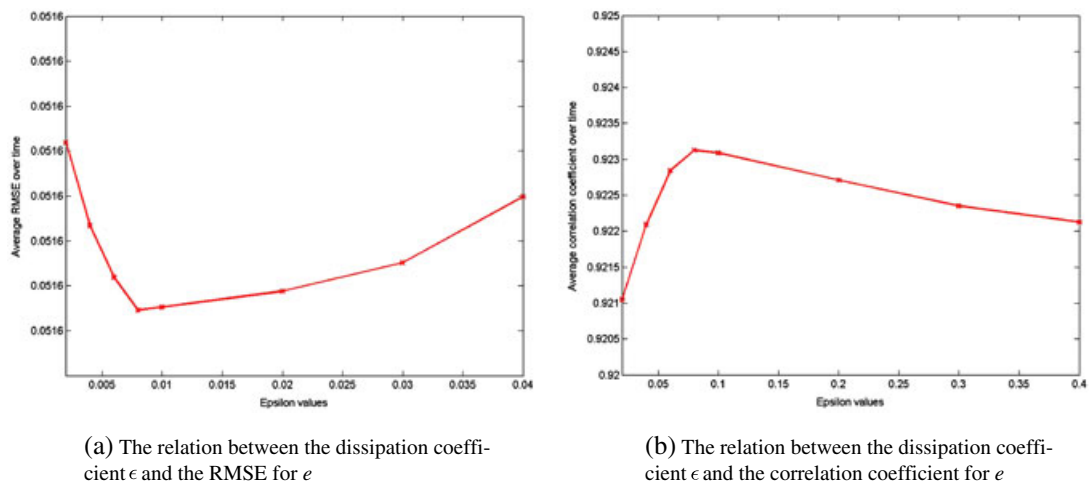


Figure 21. The variation of the (a) root mean square error (RMSE) and the correlation coefficient as a function of different values of the dissipation coefficient  $\epsilon$  ( $Re = 1200$ ).

Figure 18 presents the first six leading POD basis functions with and without  $H_1$  norm POD calibration using the optimal dissipation coefficient  $\epsilon = 1 \times 10^{-2}$ .

The full-model solutions compared with the corresponding POD reduced-order solutions for the specific energy  $e$  at the 21st and 41st  $x$ -direction nodes are shown in Figure 19.

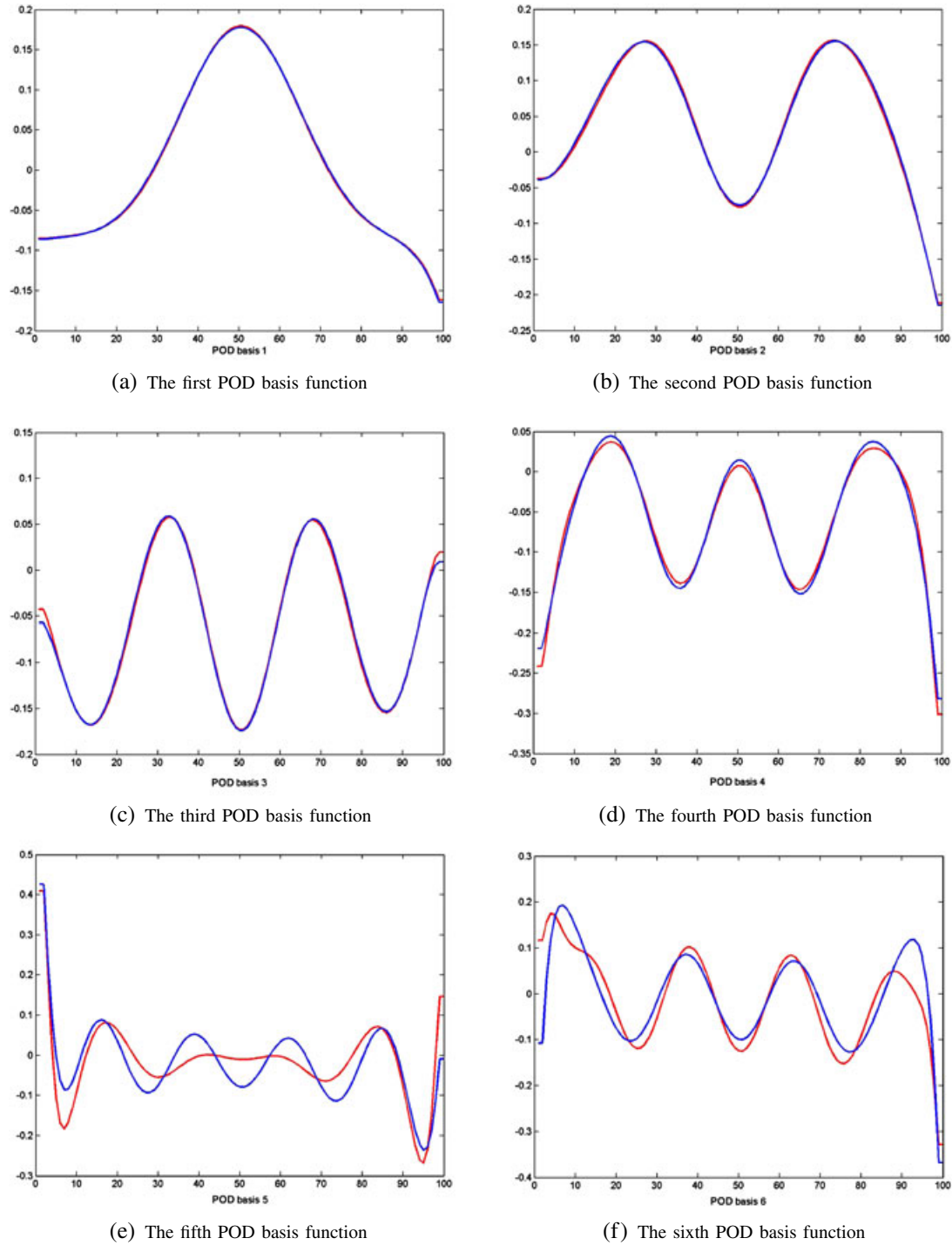


Figure 22. (a–f) The first six leading POD basis functions for  $e$  (blue: without POD calibration, red: with POD calibration using the optimal dissipation coefficient  $\epsilon = 8 \times 10^{-2}$ ) ( $Re = 1200$ ).

5.2.3.  $Re = 1.2 \times 10^3$ . We carried out the same tests for the optimal dissipation coefficient  $\epsilon$  with a higher Reynolds number of  $Re = 1.2 \times 10^3$ . The RMSE and the COR for the specific energy  $e$  corresponding to different values of  $\epsilon$  in the interval  $10^{-3} \leq \epsilon \leq 10$  and  $2 \times 10^{-2} \leq \epsilon \leq 4 \times 10^{-1}$  are presented in Figures 20 and 21, respectively. The smallest RMSE and the largest correlation number were both obtained when  $\epsilon = 8 \times 10^{-2}$ .

The first six leading POD basis functions with and without  $H_1$  norm POD calibration using the optimal dissipation coefficient  $\epsilon = 8 \times 10^{-2}$  are presented in Figure 22.

Figure 23 shows the full-model solutions compared with the corresponding POD reduced-order solutions for the specific energy  $e$  at the 21st and 41st  $x$ -direction nodes.

In conclusion, the optimal dissipation coefficient  $\epsilon$  varied as we increased the Reynolds number in the PNS equations. The optimal dissipation coefficients for the PNS model with the Reynolds number  $Re = 0.6 \times 10^3$ ,  $Re = 1 \times 10^3$ , and  $Re = 1.2 \times 10^3$  are  $1 \times 10^{-2}$ ,  $2 \times 10^{-2}$ , and  $8 \times 10^{-2}$ , respectively, which are all of the order  $10^{-2}$  and increase in magnitude as the Reynolds number becomes higher.

## 6. CONCLUSIONS AND FUTURE WORK

In this paper, a POD method is applied to derive a reduced-order model for the PNS equations. First, ensembles of snapshots were computed from transient solutions (along the  $x$  direction) obtained with the space-marching finite difference scheme, and this process can be omitted in actual applications where the ensemble of snapshots can be obtained from physical system trajectories by drawing samples from experiments and interpolation (or data assimilation). Then, we derived the POD basis functions from the ensembles of snapshots and developed the reduced-order model, in which a much smaller number of the POD basis functions make the reduced-order model optimal in the sense of energy captured. To improve the accuracy and the stability of the reduced-order model in the presence of increasingly higher Reynolds number, we applied the Sobolev  $H_1$  norm calibration to the POD method. Finally, a number of numerical experiments were carried out to demonstrate the accuracy of the POD reduced-order model compared with the full PNS model. The efficiency of the  $H_1$  norm POD calibration in the presence of high Reynolds number was demonstrated. An optimal dissipation coefficient yielding the best RMSE and COR between the full and reduced-order PNS models was estimated for several cases of various Reynolds numbers. We also tested the impact of the number of snapshots and different inflow conditions on the performance of the POD reduced-order model.

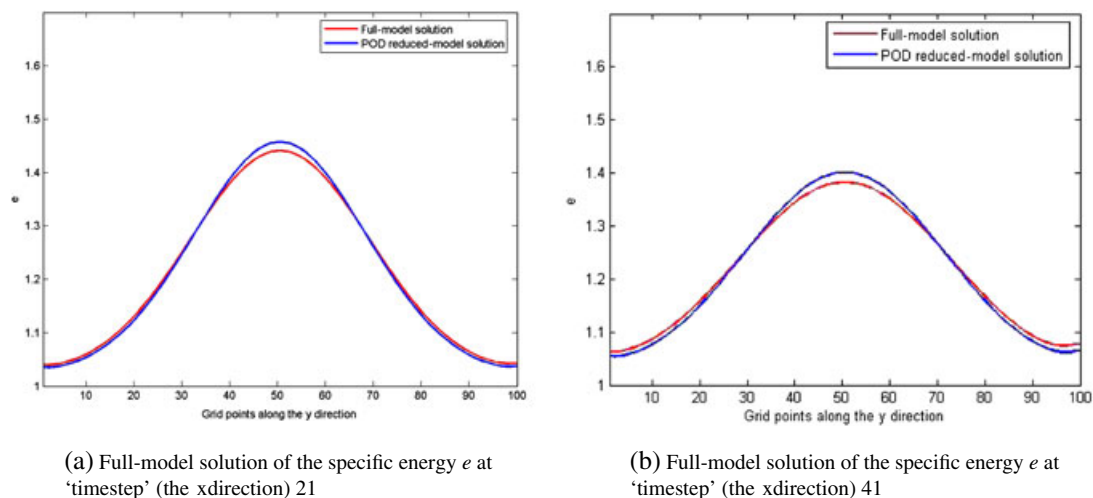


Figure 23. (a) Full-model solution and (b) POD reduced-order model solution of the PNS equations ( $Re = 1200$ ).

In a follow-up paper, we will apply the POD technique to the ill-posed inverse problem of the PNS equations [12–14] to estimate the inflow parameters from the outflow measurements of the two-dimensional supersonic laminar flow using some robust large-scale unconstrained minimization methods. The efficiency and the feasibility of the POD technique applied to the inverse problem will also be studied.

## ACKNOWLEDGEMENTS

Prof. I. M. Navon acknowledges the support of the National Science Foundation (grant ATM-0931198). Prof. Zhendong Luo acknowledges the support of the National Science Foundation of China (grant 10871022) and the Natural Science Foundation of Hebei Province (grant A2010001663). Juan Du acknowledges the support of the China Scholarship Council and the Department of Scientific Computing, which hosted her for her 1-year visit at Florida State University, FL, USA.

## REFERENCES

1. Fukunaga K. *Introduction to Statistical Recognition (Computer Science and Scientific Computing Series)*, 2nd edn. Academic Press: Boston, MA, 1990.
2. Jolliffe IT. *Principal Component Analysis*. Springer: Berlin, 2002.
3. Crommelin DT, Majda AJ. Strategies for model reduction: comparing different optimal bases. *Journal of the Atmospheric Sciences* 2004; **61**:2206–2217.
4. Majda AJ, Timofeyev I, Vanden-Eijnden E. Systematic strategies for stochastic mode reduction in climate. *Journal of the Atmospheric Sciences* 2003; **60**:1705–1723.
5. Du J, Zhu J, Luo Z, Navon IM. An optimizing finite difference scheme based on proper orthogonal decomposition for CVD equations. *Communications in Numerical Methods in Engineering* 2011; **27**:78–94.
6. Cao Y, Zhu J, Navon IM, Luo Z. A reduced order approach to four-dimensional variational data assimilation using proper orthogonal decomposition. *International Journal for Numerical Methods in Fluids* 2007; **53**:1571–1583.
7. Cao Y, Zhu J, Luo Z, Navon IM. Reduced order modeling of the upper tropical Pacific Ocean model using proper orthogonal decomposition. *Computers & Mathematics with Applications* 2006; **52**:1373–1386.
8. Anderson DA, Tannehill JC, Pletcher RH. *Computational Fluid Mechanics and Heat Transfer*. Hemisphere Publishing Corporation: New York, 1998.
9. Rubin SG, Tannehill JC. Parabolized/reduced Navier–Stokes computational techniques. *Annual Review of Fluid Mechanics* 1992; **24**:117–44.
10. Alekseev AK. On estimation of entrance boundary parameters from downstream measurements using adjoint approach. *International Journal for Numerical Methods in Fluids* 2001; **36**:971–982.
11. Fang F, Pain CC, Navon IM, Piggott MD, Gorman GJ, Farrell PE, Allison PA, Goddard AJH. A POD reduced-order 4D-Var adaptive mesh ocean modelling approach. *International Journal for Numerical Methods in Fluids* 2009; **60**:709–732.
12. Alekseev AK, Navon IM. The analysis of an ill-posed problem using multiscale resolution and second order adjoint techniques. *Computer Methods in Applied Mechanics and Engineering* 2001; **190**:1937–1953.
13. Alekseev AK. 2D inverse convection dominated problem for estimation of inflow parameters from outflow measurements. *Inverse Problems in Engineering* 2000; **8**:413–434.
14. Alekseev AK, Navon IM, Steward JL. Comparison of advanced large-scale minimization algorithm for the solution of inverse ill-posed problems. *Optimization Methods and Software* 2009; **24**:63–87.
15. Luo Z, Wang R, Zhu J. Finite difference scheme based on proper orthogonal decomposition for the non-stationary Navier–Stokes equations. *Science in China Series A: Mathematics* 2007; **50**:1186–1196.
16. Afanasiev K, Hinze M. Adaptive control of a wake flow using proper orthogonal decomposition. In *Shape Optimization and Optimal Design: Proceedings of the IFIP Conference*, Cagnol J, Polis MP, Zolesio J.-P. (eds). CRC Press: New York, 2001; 317–332.
17. Hinze M, Kunisch K. Three control methods for time-dependent fluid flow. *Flow, Turbulence and Combustion* 2000; **65**:273–298.
18. Fang F, Pain CC, Navon IM, Gorman GJ, Piggott MD, Allison PA, Farrell PE, Goddard AJH. A POD reduced order unstructured mesh ocean modelling method for moderate Reynolds number flows. *Ocean Modelling* 2009; **28**:127–136.
19. Galletti B, Bottaro A, Bruneau CH, Iollo A. Accurate model reduction of transient and forced wakes. *European Journal of Mechanics B/Fluids* 2007; **26**:354–366.
20. Iollo A, Lanteri S, Desideri JA. Stability properties of POD-Galerkin approximations for the compressible Navier–Stokes equations. *Theoretical and Computational Fluid Dynamics* 2000; **13**:377–396.
21. Cordier L, Abou El Majd B, Favier J. Calibration of POD reduced-order models using Tikhonov regularization. *International Journal for Numerical Methods in Fluids* 2009; **63**:269–296.
22. Couplet M, Basdevant C, Sagaut P. Calibrated reduced-order POD-Galerkin system for fluid flow modelling. *Journal of Computational Physics* 2005; **207**:192–220.

23. Galletti B, Bruneau CH, Zannetti L, Iollo A. Low-order modelling of laminar flow regimes past a confined square cylinder. *Journal of Fluid Mechanics* 2004; **503**:161–170.
24. Noack BR, Afanasiev K, Morzynski M, Tadmor G, Thiele F. A hierarchy of low-dimensional models for the transient and post-transient cylinder wake. *Journal of Fluid Mechanics* 2003; **497**:335–363.
25. Bourguet R, Braza M, Harran G, Dervieux A. Low-order modeling for unsteady separated compressible flows by POD-Galerkin approach. *IUTAM Symposium on Unsteady Separated Flows and Their Control*. Springer: Heidelberg, 2009.
26. Sirisup S, Karniadakis GE. A spectral viscosity method for correcting the long-term behavior of POD models. *Journal of Computational Physics* 2004; **194**:92–116.
27. Ullmann S, Lang J. A POD-Galerkin reduced model with updated coefficients for Smagorinsky LES. *ECCOMAS-CFD 2010 Fifth European Conference on Computational Fluid Dynamics*, Lisbon, Portugal, June 14–17, 2010.